J. Fluid Mech. (1992), *vol.* 236, *pp.* 579–605
Printed in Great Britain

Low-Reynolds-number effects in a fully developed turbulent channel flow

By R. A. ANTONIA[1], M. TEITEL[1], J. KIM[2] AND L. W. B. BROWNE[1]

[1] Department of Mechanical Engineering, University of Newcastle, New South Wales, 2308, Australia

[2] Center for Turbulence Research, NASA-Ames Research Center, Moffett Field, CA 94035, USA

(Received 25 June 1990 and in revised form 10 September 1991)

Low-Reynolds-number effects are observed in the inner region of a fully developed turbulent channel flow, using data obtained either from experiments or by direct numerical simulations. The Reynolds-number influence is observed on the turbulence intensities and to a lesser degree on the average production and dissipation of the turbulent energy. In the near-wall region, the data confirm Wei & Willmarth's (1989) conclusion that the Reynolds stresses do not scale on wall variables. One of the reasons proposed by these authors to account for this behaviour, namely the 'geometry' effect or direct interaction between inner regions on opposite walls, was investigated in some detail by introducing temperature at one of the walls, both in experiment and simulation. Although the extent of penetration of thermal excursions into the opposite side of the channel can be significant at low Reynolds numbers, the contribution these excursions make to the Reynolds shear stress and the spanwise vorticity in the opposite wall region is negligible. In the inner region, spectra and co-spectra of the velocity fluctuations u and v change rapidly with the Reynolds number, the variations being mainly confined to low wavenumbers in the u spectrum. These spectra, and the corresponding variances, are discussed in the context of the active/inactive motion concept and the possibility of increased vortex stretching at the wall. A comparison is made between the channel and the boundary layer at low Reynolds numbers.

1. Introduction

The fully developed turbulent flow between parallel walls has received a great deal of attention, both in experiment (e.g. Laufer 1950; Comte-Bellot 1965) and, more recently, direct numerical simulation (Kim, Moin & Moser 1987; Lyons, Hanratty & McLaughlin 1989) at relatively small Reynolds numbers. One reason for this interest is the relatively simple flow geometry and the consequent simplifications to the governing equations of motion. The resulting balance between the streamwise pressure gradient and the gradient, in a direction normal to the walls, of the Reynolds shear stress has, inter alia, been used to calibrate wall shear stress gauges. Another reason lies in the often made assumption that the structure of turbulence near a wall is universal so that any knowledge about coherent structures or organized aspects of the motion near a duct wall is of direct relevance to the near-wall region of a boundary layer.

In support of the previous assumption is the similarity between the vortical structures in the two flows (e.g. Kim & Moin 1986; Wallace 1982). This is of some

interest given the differences which exist between the outer regions of the two flows. The turbulent/non-turbulent interface, an important feature of the boundary layer, is absent in the duct. On the other hand, the possibility of an interaction between the back-to-back shear layers near the duct centreline cannot exist in the boundary layer. Reynolds number effects in the outer part of the boundary layer have been associated with the viscous superlayer (Huffman & Bradshaw 1972; Murlis, Tsai & Bradshaw 1982), which occupies a larger fraction of the outer layer at lower Reynolds numbers. Such effects should be absent in the duct, owing to the absence of the superlayer.

Huffman & Bradshaw (1972) argued that the outer layer and outer boundary conditions affect the inner layer primarily via the shear stress gradient $\partial\tau/\partial y$ (τ is the total shear stress $-\overline{uv}+\nu\partial\bar{U}/\partial y$, ν is the kinematic viscosity). In this paper, x, y, z denote streamwise, normal (to the wall) and spanwise directions respectively; u, v, w denote velocity fluctuations in the x, y, z, directions respectively. The shear stress gradient is small in the inner region of a constant pressure boundary layer, but not in a fully developed duct flow where it is balanced by the pressure gradient $\mathrm{d}p/\mathrm{d}x$. El Telbany & Reynolds (1980, 1981) included $\partial\tau/\partial y$ in their dimensional arguments for both the mean velocity and turbulence intensities in duct flows. For a fully developed duct flow, $|\partial\tau^+/\partial y^+|$ is the inverse of the Reynolds number h^+ ($\equiv hU_\tau/\nu$, where the superscript + denotes normalization by wall variables and h is the duct half-width). This Reynolds number (sometimes denoted as the Kármán number) can be interpreted as the ratio of an outer lengthscale (h) and an inner lengthscale (ν/U_τ).

Spalart (1988) investigated low-Reynolds-number effects in a turbulent boundary layer for zero pressure gradient using direct numerical simulations for values of R_θ ($\equiv U_1\theta/\nu$, U_1 is the free-stream velocity and θ the momentum thickness) extending up to 1410. Near the wall, the normal stresses $\overline{u^2}, \overline{w^2}$, the r.m.s. pressure and r.m.s. vorticity components did not scale on wall variables. The increase with R_θ of these quantities (normalized on wall variables) was attributed to the inactive motion (Townsend 1961; Bradshaw 1967).

Wei & Willmarth (1989, hereinafter referred to as WW) have measured the velocity components u and v with a laser-Doppler anemometer system in a turbulent channel flow over the range $3000 \leqslant Re \leqslant 40000$, where $Re = U_0 h/\nu$ (U_0 is the velocity at the centreline). In the inner region, distributions of u'^+, v'^+ (a prime denotes the r.m.s. value, i.e. $u' \equiv \overline{u^2}^{\frac{1}{2}}$) and $\overline{u^+v^+}$ showed a (generally) systematic dependence on Re. They hypothesized that this dependence on Re is caused by changes in the structure of turbulence close to the wall and suggested two possible reasons for these changes. The first of these is an increase (with Re) in vortex stretching of the inner region, the increase being larger than expected if wall scaling were applicable. The second relates to the possibility that inner region structures from opposite walls do in fact interact, especially at low Reynolds numbers. It was speculated that, when the Reynolds number is low, an ejection occurring near one wall may extend well across the centreline to the opposite wall so that there may be a constant exchange of counter-rotating fluid between the inner regions of the two walls. These authors referred to this phenomenon as the 'geometry effect' (the term appears to have first been mentioned by Sabot & Comte-Bellot 1976, in the context of turbulent pipe flow). No direct evidence was provided for the geometry effect, apart from a comparison between instantaneous uv signals obtained at approximately the same y^+ location (≈ 125) but at different Reynolds numbers ($Re = 2970$ and 22776). At the higher Reynolds number, the y location may be assumed to be in the inner region ($y/h = 0.13$) while, at the lower Reynolds number, this location ($y/h = 0.73$) is

sufficiently close to the duct centreline to expect fluid incursions with an opposite-signed shear stress.

The main evidence for the 'vortex stretching' suggestion was provided by the increase with Reynolds number in the high wavenumber parts of the u-spectrum and more especially the v-spectrum at $y^+ \approx 15$. It was argued that an increase of vorticity in the legs of the hairpin vortices – which are aligned primarily in the streamwise direction close to the wall – would result in a significant increase in v (and presumably also w – although this quantity was not measured) and a smaller increase in u.

Since the geometry effect does not appear to have been taken into account in most turbulent duct flow investigations it seems important (as noted by WW) that results previously obtained for this flow should be re-interpreted in the light of this effect. Also, because the effect is absent in a boundary layer, one might expect differences between the inner regions of a boundary layer and a duct. Differences in the mean velocity distribution over the buffer region were reported by Reynolds & El Telbany (1982). With respect to the possible importance of the geometry effect, Dean & Bradshaw (1976) found that, following the merging of the boundary layers in the entrance region of the duct, large-scale three-dimensional eruptions associated with the opposite shear layers can cross the duct centreline. They referred to a 'time-sharing' of the central duct region by the eruptions from the opposite shear layers. Apart from this time-sharing, these authors assumed that to a first approximation there was no significant interaction between opposite eruptions. Bradshaw, Dean & McEligot (1973) reported good agreement between experiments and a calculation using the same empirical input as in a boundary layer but assuming that the turbulence fields on either side of the duct can be superposed. Recently, Teitel & Antonia (1990) showed that the extent of penetration of one shear layer into the opposite side is in fact greater than suggested by Dean & Bradshaw. This penetration was also evident in space–time correlations of v. Using a quadrant analysis applied to the product uv, it was noted that ejection-type events associated with one wall could occasionally reach the opposite near-wall region, the average extent of penetration increasing as the Reynolds number decreased or as the strength of the events increased. The total contribution these events made to $\overline{uv}$ in the opposite near-wall region was not however estimated and hence no insight was gained into how important these incursions are in the context of the opposite near-wall region.

In this paper, we first present new data in the duct – obtained both by experiment and DNS – and examine the evidence for the Reynolds-number dependence, concentrating mainly on the inner region. We next assess the two main reasons for the Reynolds-number dependence that were suggested by WW. Evidence of the penetration of temperature-marked fluid from the inner region of one wall into the corresponding region of the opposite wall is considered, using both types of data, in §5. Spectra of u, v and the uv co-spectra in the inner region are also examined (§6) to assess the relative importance of: (i) vortex stretching at high wavenumbers; and (ii) the 'inactive' motion at low wavenumbers. A brief comparison in terms of Reynolds number effects, between the duct and the boundary layer is finally presented (§7).

2. Experimental details

Measurements were made in a fully developed duct flow at four values of Re in the range 3300–21 500. The duct aspect ratio of 18 is sufficiently large to ensure two-dimensionality of the mean flow. The measurement station is located at a distance

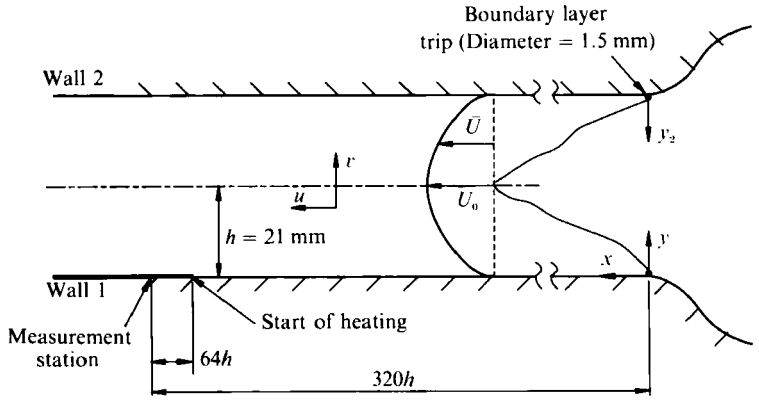

FIGURE 1. Duct configuration and definitions.

Re	U_τ (m/s)	h^+	Centreline velocity U_0 (m/s)	U_0/U_τ	Wire length l_w^+ (l_w = 0.29 mm)	Kolmogorov lengthscale η (mm) at $y^+ \approx 32$	l_w/η at $y^+ \approx 32$
3300	0.133	181	2.43	18.27	2.52	0.22	1.32
5000	0.183	256	3.57	19.51	3.47	0.16	1.81
11600	0.380	525	8.40	22.10	7.22	0.07	4.14
21500	0.648	916	15.20	23.46	12.32	0.04	7.25

TABLE 1. Experimental conditions in the duct

$x = 320h$ from the entrance to the working section (h is 21 mm). Two boundary-layer trips of 1.5 mm in diameter were placed at the entrance to the duct, one on each wall, spanning the complete height of the duct. All the checks that were made (details are given by Shah 1988) indicated that the flow was fully developed at $x = 320h$.

A single X-probe was traversed across the duct at the measurement station. The probe was built using 1.27 μm Wollaston Pt-10% Rh wires (length ≈ 0.3 mm; lateral separation ≈ 0.3 mm). The wires were operated at an overheat ratio of 1.4 with in-house constant temperature circuits. Direct current offset voltages were applied to the signals from these circuits before amplification and low-pass filtering at a cut-off frequency of 4.8 kHz/channel. They were then digitized on a PDP 11/34 computer using a 12-bit A/D data acquisition system at a sampling frequency of 10 kHz/channel.

The X-probe was mounted on a traversing mechanism with a least count of 0.01 mm. The initial distance of the X-probe to the wall was determined using a theodolite and the reflection method. Velocity and yaw calibrations of the X-probes were done at the centre of the duct. The plane of the X-probe was in the spanwise or (x, z)-plane for yaw calibration and in the (x, y)-plane when velocity calibrations and (u, v) measurements were made (see figure 1 for coordinate axes). For these calibrations, a Pitot tube, connected to a Baratron pressure transducer, was placed on the duct centreline. The transducer output and the outputs from the constant-temperature bridges were digitized at a sampling frequency of 10 Hz/channel using a data logger/personal computer.

Some comments need to be made in connection with the choice of the X-probe geometry and wire selection in the present experiments. First, in order to maximize

the spatial resolution, it was decided to use 1.2 μm dia. wires. Wire lengths of about 0.3 mm ensured that the length to diameter ratio was at least 200 while the wire length remained relatively small in terms of wall units. Table 1 shows that the latter requirement is adequately satisfied at the lower Reynolds numbers; the ratio of wire length to Kolmogorov lengthscale $\eta \equiv \nu^{\frac{3}{4}}/\bar{\epsilon}^{\frac{1}{4}}$ (where $\bar{\epsilon}$ is the average turbulent energy dissipation) at $y^+ \approx 32$ is also satisfactory at these Reynolds numbers. Since velocity derivatives were not measured, $\bar{\epsilon}$ was estimated using the direct numerical simulation value of the ratio of production to dissipation of turbulent energy reported by Mansour, Kim & Moin (1989) and the measured production value. The position $y^+ \approx 32$ was chosen as it is the smallest y^+ for which measurements could be made at $Re = 21500$. Table 1 shows that the ratio l_w/η is significant at the larger Reynolds numbers.

The second comment relates to the adequacy of a 90° angle between the wires when measurements were made near a wall. In this region, the local mean velocity is low and the angle that the instantaneous velocity vector makes to the X-probe may become comparable or even exceed half the included angle between the wires. This problem was addressed in the case of a boundary layer near a rough wall by Perry, Lim & Henbest (1987). They found that the use of a 90° probe underestimated v' and $\overline{uv}$ by comparison to a 120° probe or a flying X-probe. At $Re = 3300$, which represents the worst condition in terms of small absolute values of $\bar{U}$, it was found that, at $y^+ \approx 10$, the minimum and maximum values of the vector angle $[\beta \equiv \tan^{-1} v/(\bar{U}+u)]$ were $-35°$ and $+30°$ respectively. This range of values (the maximum value of β' was 5°) suggests that fluctuations of the velocity vector in the (x, y)-plane should be adequately resolved by the present 90° X-probe.

Another source of error in X-probe measurements is the contamination by the w fluctuation (e.g. Perry *et al.* 1987). Investigation of this effect seems difficult experimentally although, for the present experiments, we established, by operating one of the X-probe wires in a constant current (0.1 mA) circuit as a temperature sensor, that there was no cross-talk between the wires. Moin & Spalart (1987) used a numerical database to evaluate the response of an X-probe in a turbulent boundary layer. They concluded that errors caused by neglecting w were important (generally larger than those caused by linearized calibration or axial cooling). An opposite conclusion was reached by Suzuki & Kasagi (1990) using their own direct numerical simulation database of a two-dimensional turbulent channel flow ($h^+ = 150$). They found that the effect of w was negligible while the lateral (spanwise) spacing Δz between the X-wires caused v'^+ to be overestimated in the near-wall region.

3. Direct numerical simulation details

Direct numerical simulations (DNS) of fully developed duct flow were performed at $Re = 3300$ and 7900. The numerical algorithm and other details used to perform the simulations can be found in Kim *et al.* (1987). For the $Re = 3300$ case, $128 \times 129 \times 128$ (in the x, y, z directions respectively) spectral modes were used in the computation. The spacings between collocation points in the streamwise and spanwise directions were $\Delta x^+ \approx 11$ and $\Delta z^+ \approx 4$. Non-uniform meshes were used in the normal direction, with the minimum spacing $\Delta y^+ \approx 0.05$ at the wall and the maximum spacing $\Delta y^+ \approx 4.4$ at the centreline. For the $Re = 7900$ case, $256 \times 193 \times 192$ (in the x, y, z directions respectively) spectral modes were used in the computation, which gave roughly the same collocation grid spacings ($\Delta x^+ \approx 7$, $\Delta z^+ \approx 4, \Delta y^+ \approx 0.05$–5.5) as for $Re = 3300$. At both Reynolds numbers, the grid

resolutions in the horizontal directions may seem inadequate, given that the estimated Kolmogorov lengthscales in this flow are of the order of 1.5 to 42 wall units (no dependence of the Kolmogorov lengthscale on Re was found). Various statistics, such as the energy and dissipation spectra, energy budgets for the Reynolds stress equations, and other higher-order statistics, were examined to make sure that the new computation at the high Reynolds number was not affected from inadequate grid resolution. In addition, several instantaneous velocity and vorticity fields were carefully examined to see whether there was any evidence of poor resolution that might not have emerged from the computed statistics. As a result of these checks, it was concluded that the computed flow fields at $Re = 7900$ should be as reliable as those at $Re = 3300$.

After the velocity field reached a statistically steady state, the lower wall was heated at a constant temperature. The temperature was a passive scalar, i.e. temperature fluctuations were assumed to have no effect on the velocity field. The temporal evolution of the temperature field can be interpreted in terms of a spatial evolution, as in the case of the experiment described in §5.

Statistics associated with the temperature field presented in this paper were obtained from the computed flow field at $t^+ \equiv tU_\tau^2/\nu = 516$, where $t^+ = 0$ corresponds to the time when the heat was introduced at the lower wall.

4. Mean velocity and turbulence intensities

Mean velocity distributions, measured with the X-probe, are shown in figure 2. It is difficult to discern any systematic dependence on Re in the region $y^+ \lesssim 100$, allowing for the experimental uncertainty. The measurements are in good agreement with those obtained by Shah (1988) in the same duct with a single hot wire. They are also in reasonable agreement with the WW profiles; to avoid crowding, these have not been included in figure 2. The DNS profiles are also in reasonable agreement with the measurements: they are, however, shown separately in figure 3 as they indicate a small difference between $Re = 3300$ and $Re = 7900$. The Reynolds-number dependence in figure 3 is consistent, however, with the trend of the mean velocity profiles measured by Patel & Head (1969) and analysed by Huffman & Bradshaw (1972). The latter authors found that the log-law remains valid in a wide range of low-Reynolds-number flows provided the dimensionless shear stress gradient $|\partial\tau^+/\partial y^+|$ is not much greater than about 10^{-3}. This corresponds to $h^+ \gtrsim 1000$. At lower Reynolds numbers, the best fit to the Kármán constant remained at 0.41 but the Van Driest damping length constant A^+, which essentially determines the additive constant in the log-law, increased as h^+ decreased. Reasonable fits to the profiles in figure 3 are obtained (though not shown here) with $A^+ = 28$ ($h^+ = 390$) and 33 ($h^+ = 180$), these latter values being in reasonable agreement with those obtained by Huffman & Bradshaw (1972) from their analysis of Patel & Head's (1969) data.

For $y^+ \gtrsim 10$, there is a generally systematic increase in u'^+ with Re at any given y^+ (figure 4). There is a tendency, as Re increases, for u'^+ to decay less rapidly with y^+ for $y^+ \gtrsim 30$. This trend is consistent with observations in the boundary layer (e.g. Purtell, Klebanoff & Buckley 1981). A region where u'^+ is constant (with respect to y^+) is not, however, achieved. There is reasonable agreement between DNS and experiment at $Re = 3300$. The DNS curve for $Re = 7900$ falls somewhere between the $Re = 5000$ and $Re = 11600$ experimental distributions. WW suggested that inner scaling may be valid for $y^+ < 15$. This question cannot satisfactorily be resolved by the experimental data in view of the excessive uncertainty in this region (see, for

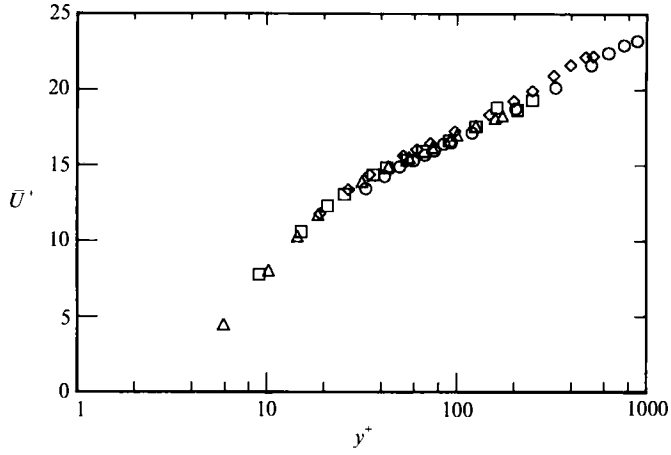

FIGURE 2. Measured mean velocity distributions. △, $Re \doteq 3300$; □, 5000; ◇, 11600; ○, 21500. These symbols are used in subsequent figures.

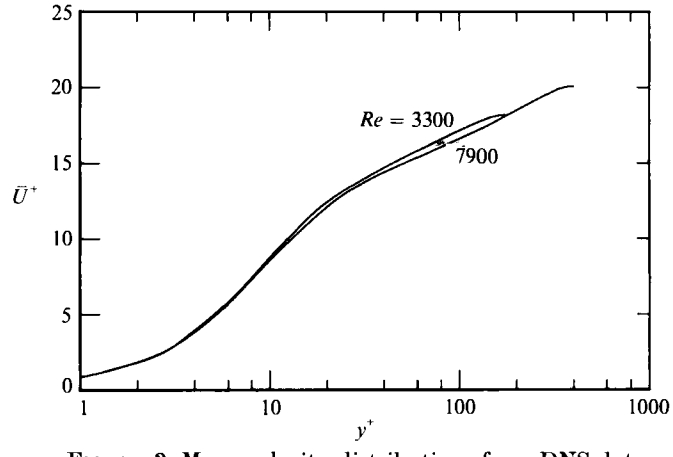

FIGURE 3. Mean velocity distributions from DNS data.

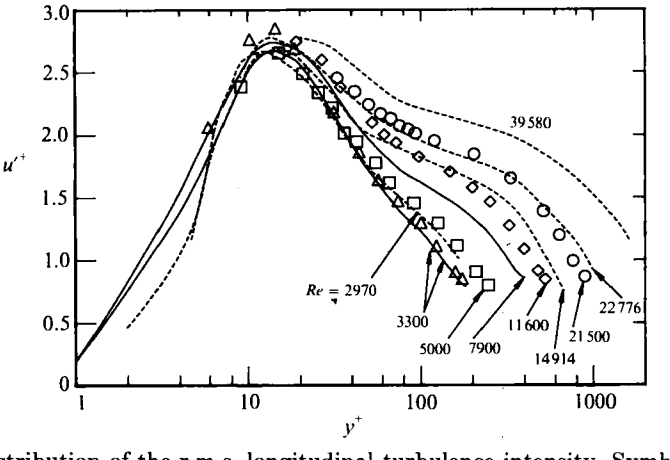

FIGURE 4. Distribution of the r.m.s. longitudinal turbulence intensity. Symbols are for present experiments. ---, Wei & Willmarth (1989); ——, DNS.

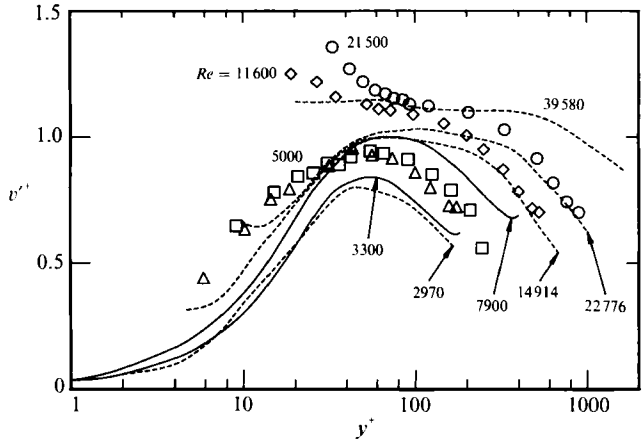

FIGURE 5. Distributions of the r.m.s. normal turbulence intensity. Symbols are for present experiments. ---, Wei & Willmarth (1989); ——, DNS.

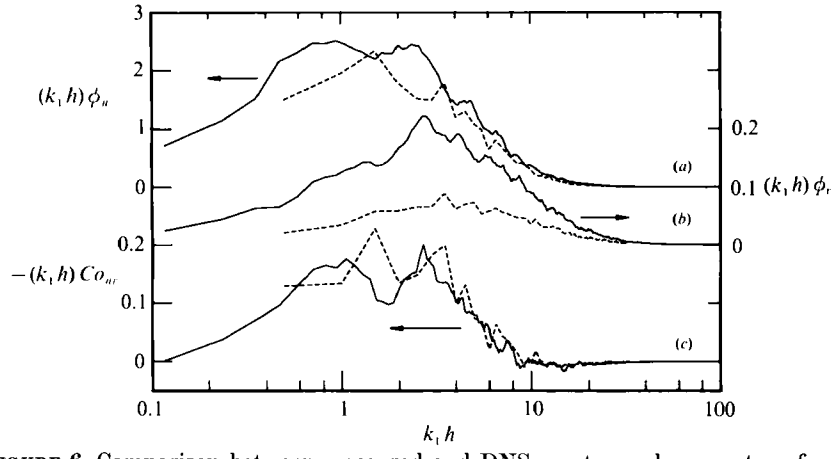

FIGURE 6. Comparison between measured and DNS spectra and co-spectra of u and v at $y^+ \approx 15$ ($Re = 3300$). ——, experiment; ---, DNS.

example, Coles 1978). The DNS data (figure 6) do indicate, however, that there are discernible differences between $Re = 3300$ and $Re = 7900$ which extend to the viscous sublayer.

The shape of the v'^+ distributions (figure 5) is quite different to that for u'^+ but the increase in v'^+ with Re reflects that displayed by u'^+. The distribution of v'^+ exhibits a plateau, the extent of which increases with Re. The agreement between experiment and DNS is not as good for v'^+ as for u'^+. For $Re \approx 3300$, there is close agreement between WW and DNS but the present experimental values (which are in reasonable agreement with the data of Kreplin & Eckelmann 1979) are larger, especially at small y^+. The rise in v'^+ at the smallest values of y^+ for $Re = 11600$ and 21500 is probably spurious. The reason for these discrepancies is not clear. Although spatial resolution should be more problematical for v than u (the energy containing part of the v spectrum resides at higher frequencies than for the u spectrum), the results of §6 show that the effect on v'^+ is in fact small.

The overestimation of v'^+, by reference to the DNS data, is significantly larger than indicated by Suzuki & Kasagi (1990). For $\Delta z^+ = 2.5$ (which corresponds to the

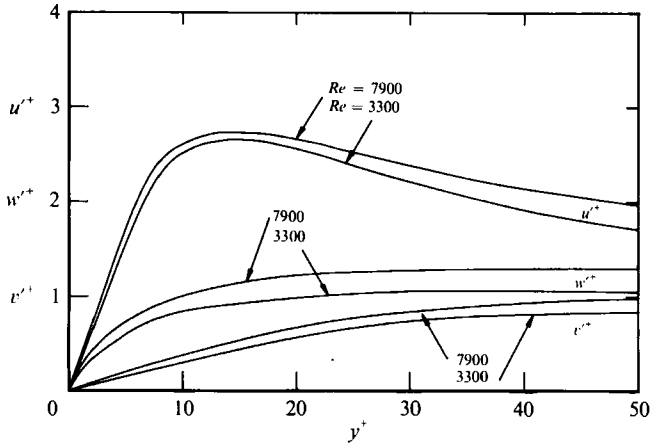

FIGURE 7. Distributions of r.m.s. turbulence intensities obtained from DNS.

present separation for $Re = 3300$), these authors estimated that the error in v'^+ was negligible for $y^+ \gtrsim 30$, but increased near the wall (at $y^+ = 10$, v'^+ is overestimated by 40%). Figure 5 suggests that the measured v'^+ is 100% larger than the DNS value at $y^+ = 10$ and remains higher everywhere in the flow.

As noted in §2, it is possible that the present v'^+ measurements may have been affected by contamination from w. This is an unresolved issue which obviously requires more investigation both experimentally and numerically (in view of the conflicting results obtained by Moin & Spalart and Suzuki & Kasagi). In order to gain some insight into the possible contamination of v, a comparison was made at various y^+ positions in the duct, between measured and DNS spectra of v of $Re = 3300$. The comparison at $y^+ \approx 15$ is presented in figure 6 where the spectra of u as well as the uv cospectra are also shown. ϕ_u and ϕ_v are the spectral densities of u and v respectively while Co represents the uv cospectrum; k_1 is the wavenumber in the x-direction in the simulation or defined by $k_1 = \omega/\bar{U}$ in the experiment (ω is the radian frequency). The normalization is such that

$$\int_0^\infty \phi_u \, \mathrm{d}k_1 = u'^{+2}, \quad \int_0^\infty \phi_v \, \mathrm{d}k_1 = v'^{+2}, \quad \int_0^\infty Co_{uv} \, \mathrm{d}k_1 = \overline{u^+v^+}. \tag{1}$$

Figure 6 indicates reasonable agreement for ϕ_u and Co_{uv} (this is maintained at all y^+ locations), irrespective of wavenumber. In the case of ϕ_v, the discrepancy is not localized in the wavenumber domain but spread over nearly the full wavenumber range. At larger y^+ locations (not shown here) there is reasonable agreement at small and large $k_1 h$, the major discrepancy occurring near the peak in the v-spectrum.

Although w measurements were not made, the DNS data for w'^+, shown in figure 7 for $0 < y^+ < 50$, suggest that the effect of Re is generally larger on w'^+ than on either u'^+ or v'^+.

Reynolds shear stress distributions shown in figure 8 were obtained either from the DNS data or calculated from the mean momentum equation and the measured mean velocity profiles using

$$-\overline{u^+v^+} = \left(1 - \frac{y^+}{h^+}\right) - \frac{\mathrm{d}\bar{U}^+}{\mathrm{d}y^+}. \tag{2}$$

As already noted by Sreenivasan (1990) in the context of pipe flow, figure 8 indicates no significant region where $\overline{u^+v^+}$ is constant, although there is perhaps a

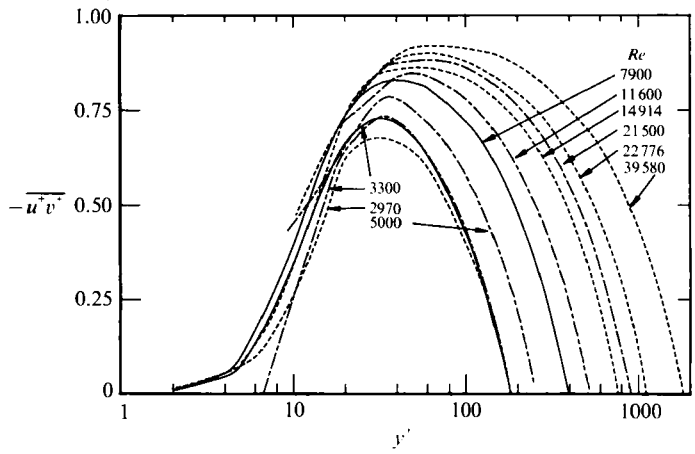

FIGURE 8. Reynolds shear stress distributions from experiment and DNS. Experimental curves are calculated using the mean momentum equation and the measured mean velocity. —·—, experiment; DNS. – – –, Wei & Willmarth (1989).

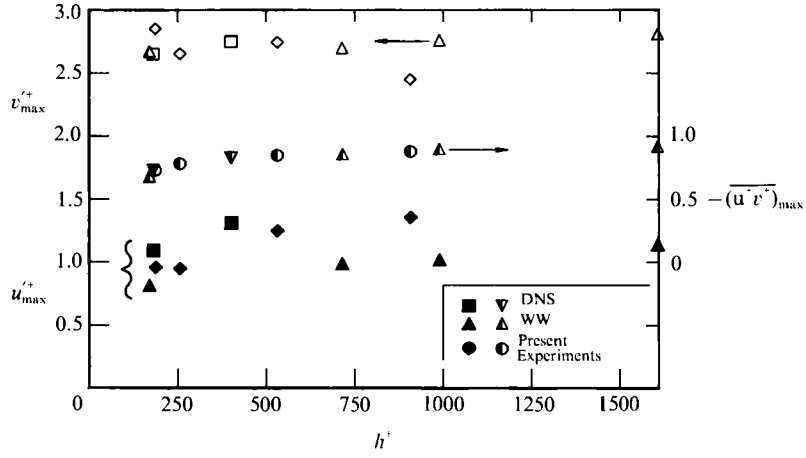

FIGURE 9. Dependence on Reynold number of the maximum r.m.s. intensities in the streamwise and normal directions and the maximum Reynolds shear stress.

tendency towards a significant plateau as Re or h^+ increases. The relation $h^+ = 0.142Re^{0.885}$, based on Dean's (1978) survey, can be used to relate h^+ to Re. The dependence of $(\overline{u^+v^+})_{max}$ on h^+ is plotted in figure 9, together with u'^+_{max} and v'^+_{max}. The magnitude of $(\overline{u^+v^+})_{max}$ approaches 0.9 at large h^+. The data for u'^+_{max} suggest that this quantity is approximately independent of h^+, as noted by Coles (1978) in his survey of duct, pipe and boundary-layer data. There are significant differences in the magnitude of u'^+_{max} between the three different data sets although each set suggests a definite increase in v'^+_{max} with h^+. The y^+ location of v'^+_{max}, notwithstanding the difficulty of defining this maximum (especially for $Re = 11600$ and 21500), increases with h^+ whereas the location of u'^+_{max} is essentially unchanged. Sreenivasan (1990) interprets this difference to mean that $\overline{v^2}$ is essentially outer-layer driven whereas $\overline{u^2}$ and hence the kinetic energy (which is dominated by $\overline{u^2}$) scale on wall variables. It is difficult to reconcile this view with the inactive motion concept (see §6).

Sreenivasan (1990) found that the y^+ location of $(\overline{u^+v^+})_{max}$ is given by

$$y^+_{max} = 2h^{+\frac{1}{2}}, \tag{3}$$

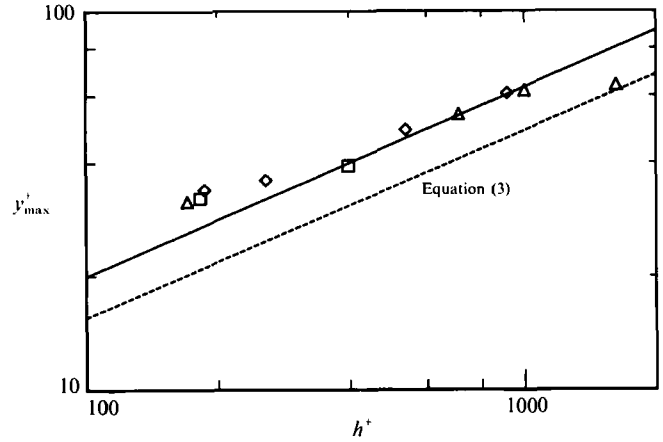

FIGURE 10. Variation with Reynolds number of y^+_{max}, the location at which $-\overline{u^+v^+}$ is maximum. ——, Sreenivasan (1990); – – –, equation (3).

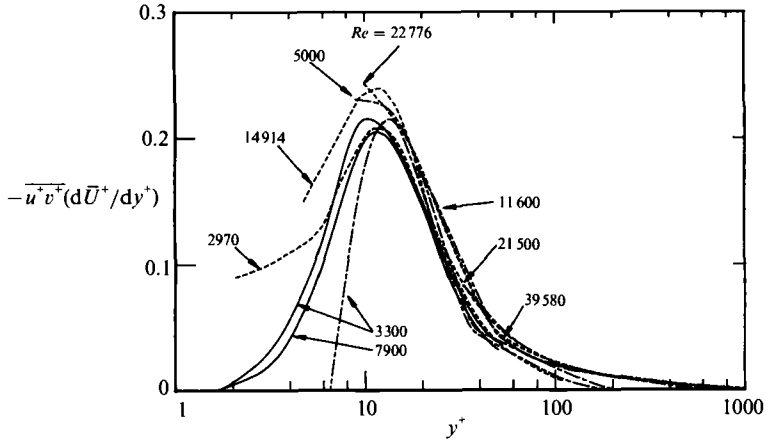

FIGURE 11. Average production of turbulent energy. Lines are as in figure 7.

for pipe, channel and boundary-layer data. The present data (figure 10) is in reasonable agreement with (3) although the present rate of increase of y^+_{max} with h^+ is slightly smaller than indicated by (3). Note that if it were assumed that $(\overline{u^+v^+})_{max}$ occurs in the logarithmic region, then $d\bar{U}^+/dy^+ = (\kappa y^+)^{-1}$ and it follows from (2) that

$$y^+_{max} = \kappa^{-\frac{1}{2}} h^{+\frac{1}{2}} \quad \text{or} \quad y^+_{max} = 1.56 h^{+\frac{1}{2}} \quad (\kappa = 0.41). \tag{4}$$

The discrepancy between (4) and (3) probably reflects the inadequacy of the assumption that y^+_{max} falls inside the log-law (y^+_{max} is only about 60 at $h^+ = 1000$).

Figure 11 indicates that scaling on wall variables provides a somewhat better collapse for the average turbulent energy production $-\overline{u^+v^+}\,d\bar{U}^+/dy^+$ than for the Reynolds stresses when $y^+ \gtrsim 15$. The large scatter in the experimental curves mainly reflects the inaccuracy in estimating $d\bar{U}^+/dy^+$. If emphasis is placed on the DNS data, their trend suggests that there can only be a slight increase in $-\overline{u^+v^+}\,d\bar{U}^+/dy^+$ with Re since the maximum theoretical value this quantity can attain is 0.25 (when $h^+ \to \infty$). (It is easy to show, starting with (2), that as $h^+ \to \infty$, the product $(-\overline{u^+v^+})\,d\bar{U}^+/dy^+$ will have a maximuum value of 0.25.) Measurements of the average energy dissipation $\bar{\epsilon}$ are difficult, especially at small y^+. For this reason, only

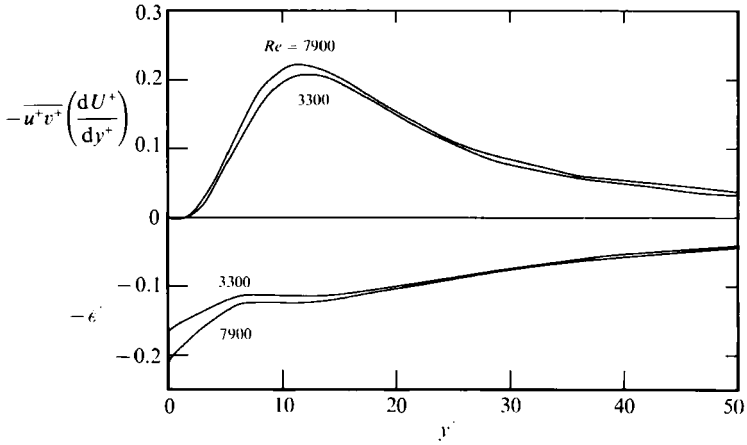

FIGURE 12. Average dissipation and production of turbulent energy in the wall region for the DNS data.

the distributions of $\bar{\epsilon}^+ (\equiv \bar{\epsilon}\nu/U_\tau^4)$ obtained from the DNS data are shown in figure 12 for the wall region (the production curves are also shown for comparison). $\bar{\epsilon}$ was calculated from estimates of all the components which appear in the definition of $\bar{\epsilon}$, namely, $\bar{\epsilon} = \nu\overline{u_{i,j}(u_{i,j}+u_{j,i})}$ where standard Cartesian tensor notation is used (here $u_{1,2} \equiv \partial u/\partial y, u_{2,3} \equiv \partial v/\partial z$, etc.). Wall scaling seems a reasonable approximation for $y^+ \gtrsim 20$. In the sublayer and buffer region, the magnitudes of production and dissipation increase with h^+. While the production must go to zero at $y^+ = 0$, the dissipation $\bar{\epsilon}^+$ has a non-zero value at the wall. The distributions in figure 12 show that the largest increase ($\approx 38\%$) in $\bar{\epsilon}^+$ occurs at the wall.

5. Interaction between opposite shear layers

To gain an idea of the extent to which fluid associated with one of the walls can penetrate across the centreline towards the opposite wall, part of one of the walls was heated slightly and an array of cold-wire temperature sensors was placed close to the other wall. As shown in figure 1, part of wall 1 was heated (at constant temperature, approximately 8 °C above ambient) starting from a distance of 1350 mm ($\approx 64h$) upstream of the measurement station. A rake of 6 cold wires was placed near wall 2. The wires were etched to a length of about 0.55 mm from 2.5 μm diameter Wollaston. The average y separation between wires was about 2 mm. The signals from the rake, shown in figure 13, indicate that temperature excursions, in excess of the ambient temperature, occur at a distance as small as $y^+ \approx 15$ from wall 2. Several observations can be made with respect to figure 13. First, the temperature excursions are usually spatially coherent suggesting that they are either due to: (*a*) an organized motion which is associated with wall 1; or to (*b*) an organized motion which is associated with wall 2 but has been marked by the temperature introduced at wall 1. Occasionally, temperature activity appears in isolation, possibly representing warm fluid which has been entrained by an organized motion associated with wall 2. The shape of the excursions suggests that the temperature rise at the downstream end (earlier time) is generally slightly steeper than the fall-off at the upstream end (later time). This ramp-like signature is opposite in sign to that expected in a turbulent boundary layer over a slightly heated wall (e.g. Chen & Blackwelder 1978; Subramanian *et al.* 1982). This signature is consistent, however, with possibility (*b*) since a heated large-scale

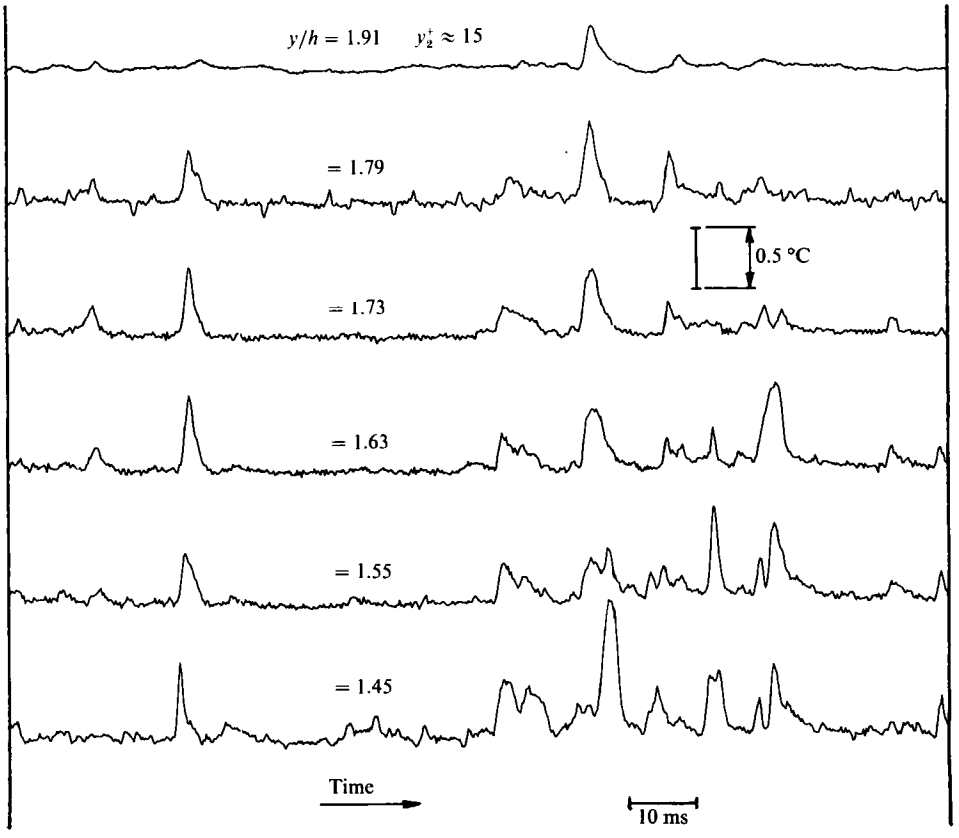

FIGURE 13. Temperature traces obtained using an array of cold wires placed near wall 2. $Re = 5000$.

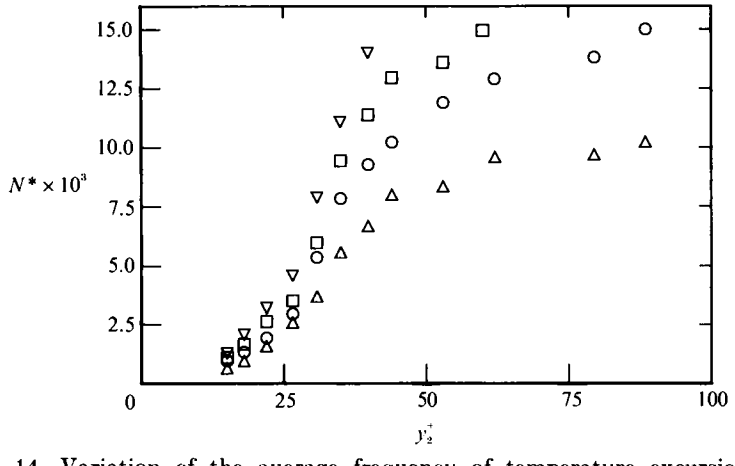

FIGURE 14. Variation of the average frequency of temperature excursions ($\theta \geqslant TH\theta'$) with distance from wall 2 for different values of the threshold TH. $Re = 3300$. ▽, $TH = 3$; □, 3.25; ○, 3.5; △, 4.

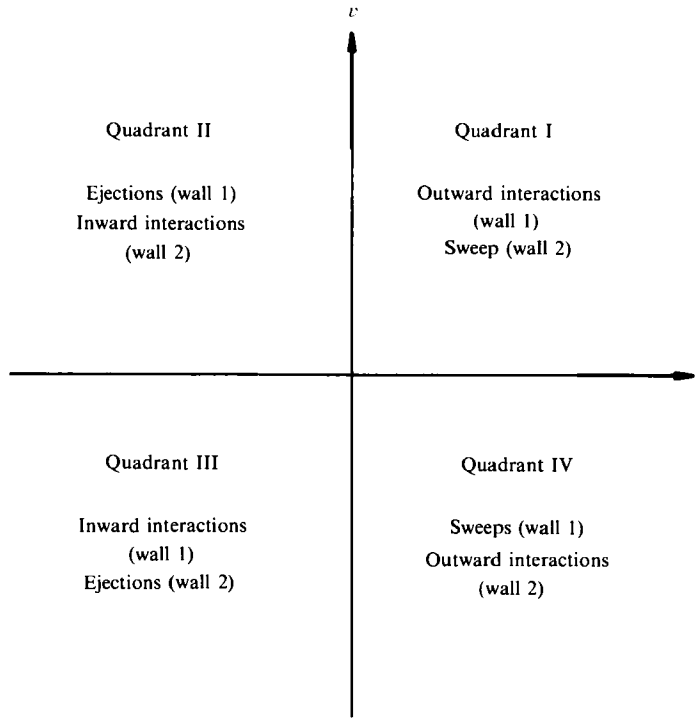

FIGURE 15. Definitions of quadrants in (u, v)-plane.

motion over a cold wall would give rise to a sudden increase in temperature at the downstream end of the motion followed by a relatively slow decrease towards ambient temperature.

The average frequency N of the thermal excursions has been obtained for a range of threshold values applied to the temperature, namely $\theta > TH\theta'$ (TH is a non-dimensional threshold). The results are shown in figure 14 for $Re = 3300$. This latter value was chosen since one might expect the penetration to be largest at this Reynolds number. The magnitude of $N^*(\equiv Nh/U_0)$ decreases as y_2^+ decreases (y_2 is measured from wall 2, figure 1). Note that the magnitude of N^* is quite small, compared for example, with the peak frequency (≈ 0.32, when normalized by h and U_0) in the v-spectrum near the centreline. The rate of decrease of N^* with y_2^+ becomes smaller as TH increases. This trend would be consistent with stronger wall 1 events penetrating further into wall 2 region than weaker events (for the present purpose, an event is defined as a fluid motion characterized by the u–v quadrant decomposition of figure 15). It is also consistent with stronger sweep-like events associated with wall 2 reaching smaller values of y_2^+ than weaker sweep-like events. It could be inferred from the trend of the data (figure 14) that excursions may actually reach wall 2. This is not the case, however, as a single cold wire mounted on a wall plug (at $y^+ \approx 5$) failed to detect any temperature excursions. It would appear that even the strongest events cannot quite reach the opposite wall at this x location although the temperature must eventually reach the wall at sufficiently large x. If it is conjectured that the sweep-like motion associated with wall 2 is marked by temperature, the expectation of finding temperature excursions at wall 2 would be reasonable since the importance of sweep-like events in the near-wall region is well documented (e.g. Kline & Robinson 1990). Although this does not occur at this station, it does not

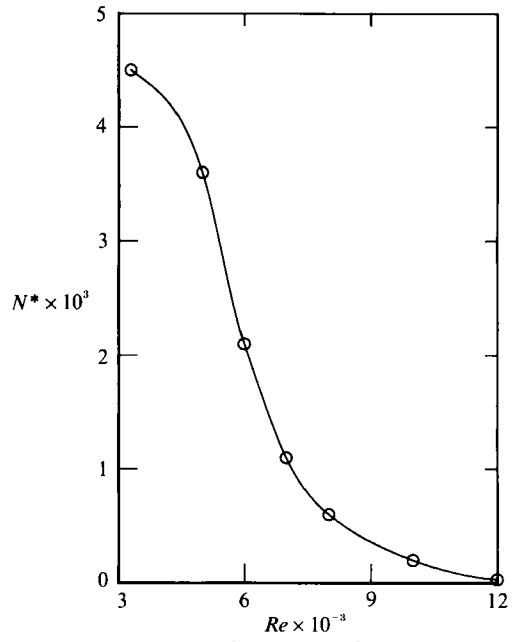

FIGURE 16. Variation of the average frequency of temperature excursions ($\theta \geqslant 3.5\theta'$) with Reynolds number ($y/h = 1.83$).

necessarily mean that temperature only marks the organized motion which is associated with wall 1. To quantify the Reynolds-number dependence of thermal excursions into the wall 2 region, the frequency with which θ exceeds $3.5\theta'$ is plotted in figure 16 for $y/h = 1.83$. Practically no excursions occurred for $Re > 10^4$. The frequency however increases as Re decreases, implying an increase in the penetration depth of the excursions as Re decreases. (Note that this increase would have been more pronounced if the measurements had been made at $y_2^+ =$ constant instead of $y/h =$ constant).

As noted in §3, temperature was introduced (wall 1) in the DNS at $t^+ = 0$ and the data were examined at $t^+ = 516$. This time corresponds to a distance of about $57h$ (compared with $64h$ in the experiment), if $U_0 (\approx 20U_\tau)$ is chosen as the convection velocity. The previous distances would be approximately halved if the convection velocity ($\approx 10.6U_\tau$) of internal shear layers in the near-wall region (Johansson, Alfredsson & Kim 1987) is used. Conventional contributions to $\overline{u^+v^+}$ were first estimated for each of the four quadrants of the (u, v)-plane. As noted by Sabot & Comte-Bellot (1976), each quadrant can be identified with events associated with both walls. For example, quadrant I may be identified with wall 2 sweeps as well as outward interactions associated with wall 1 (figure 15). Figure 17 shows the conventional contributions from each quadrant to $\overline{u^+v^+}$ as a function of y/h across the full width of the duct. Here the average in any quadrant i (I to IV) is identified by $(\overline{u^+v^+})_i$ so that

$$\sum_{i=1}^{\text{IV}} (\overline{u^+v^+})_i = \overline{u^+v^+}.$$

Near wall 1, the major contributors to $\overline{u^+v^+}$ are quadrants II and IV with relatively smaller opposite-sign contributions from the other two quadrants. At the centreline

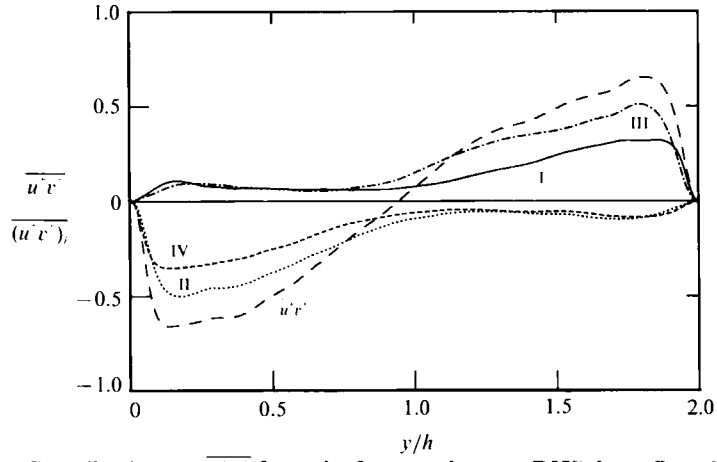

FIGURE 17. Contributions to $\overline{u^+v^+}$ from the four quadrants. (DNS data, $Re = 3300, t^+ = 516$). ——, $i = \mathrm{I}$; ....., $i = \mathrm{II}$; —·—, $i = \mathrm{III}$; – – –, $i = \mathrm{IV}$; ——, $\overline{u^+v^+}$.

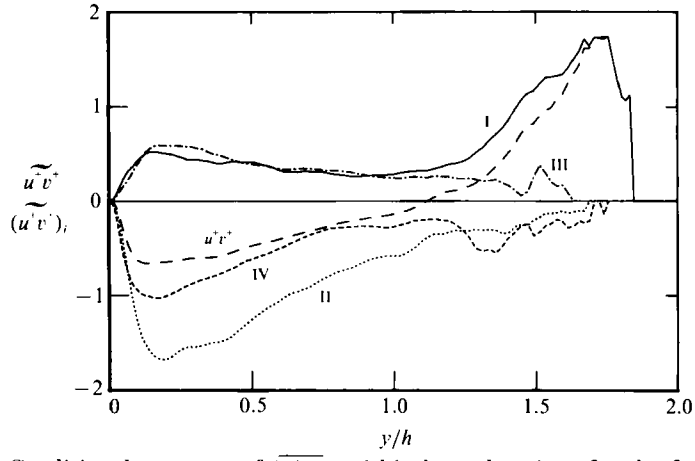

FIGURE 18. Conditional averages of $(\overline{u^+v^+})_i$ within heated regions for the four quadrants. (DNS data, $Re = 3300, t^+ = 516$). ——, $i = \mathrm{I}$; ....., $i = \mathrm{II}$; —·—, $i = \mathrm{III}$; – – –, $i = \mathrm{IV}$; ——, $\overline{u^+v^+}$.

$(y/h = 1)$, symmetry requires that $(\overline{uv})_{\mathrm{II}} = (\overline{uv})_{\mathrm{III}}$ and $(\overline{uv})_{\mathrm{I}} = (\overline{uv})_{\mathrm{IV}}$. (The departure from symmetry and lack of smoothness of the curves are due mainly to the fact that these statistics are obtained from a single velocity field at $t^+ = 516$).

Conditional averages (denoted by a tilde) of the product uv in the heated fluid regions are shown in figure 18 for each quadrant. The condition used was that the instantaneous temperature had to exceed 5% of the heated wall temperature. (This criterion was thought adequate for the present purpose as it yielded a conditionally averaged value of $v\theta$ which was approximately equal to $\overline{v\theta}$). All contributions are zero for $y/h \gtrsim 1.85$ (or $y_2^+ \lesssim 27$) as temperature excursions did not extend beyond this point. In the region $1.25 \lesssim y/h \lesssim 1.85$, the largest conditional average is associated with quadrant I and is larger than in the region $0 < y/h \lesssim 1.25$. This trend (and visual observations of u and v traces associated with thermal excursions which originate near wall 1) suggest that wall 1 ejections may, as they cross the centreline, be identified with wall 1 outward interactions or, alternately, with wall 2 sweeps (since this motion may originate in the centreline region of the duct and it is possible for it to be marked by temperature). Smaller, roughly equal, contributions are

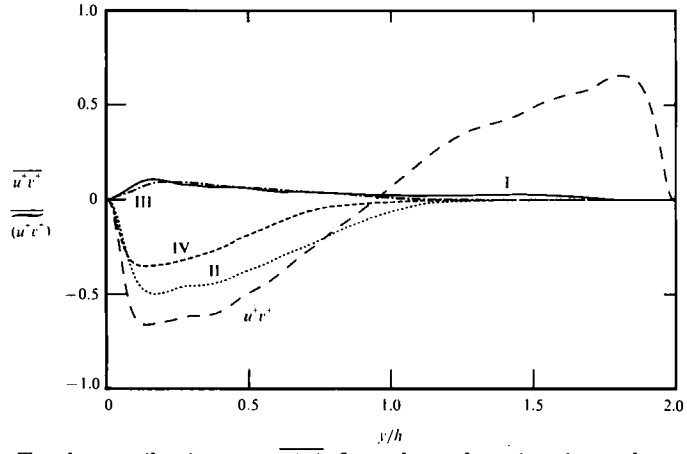

FIGURE 19. Total contributions to $\overline{u^+v^+}$ from heated region in each quadrant. (DNS data, $Re = 3300, t^+ = 516$). ——, $i = \mathrm{I}$; ....., $i = \mathrm{II}$; —·—, $i = \mathrm{III}$; – – –, $i = \mathrm{IV}$; ——, $\overline{u^+v^+}$.

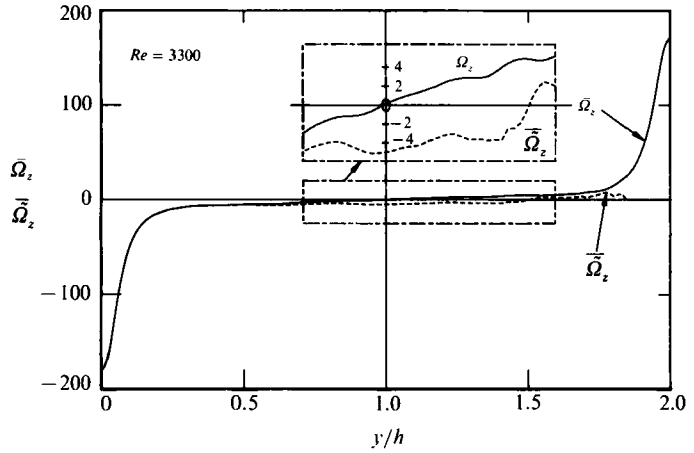

FIGURE 20. Distribution of mean spanwise vorticity $\bar{\Omega}_z$ and contribution to $\bar{\Omega}_z$ from heated region. (DNS data, $Re = 3300, t^+ = 516$). ——, $\bar{\Omega}_z$ (conventional); – –, $\tilde{\bar{\Omega}}_z$.

provided by the other quadrants. The (negative) quadrant II average vanishes at $y/h \approx 1.75$, implying that either wall 1 ejection-like events protrude a significant distance into the wall 2 region or, alternatively, the temperature marks the inward interaction events associated with wall 2. The total contribution that these excursions make to $\overline{u^+v^+}$ is obtained by multiplying the conditional average with the fraction of time occupied by these excursions. Figure 19 shows that the contribution from quadrant II is negligible for $y/h \gtrsim 1.25$ whereas the contribution from quadrant I can be distinguished up to $y/h \approx 1.75$ but its magnitude is small by comparison to $\overline{uv}$. The results for figures 18 and 19 suggest that although ejection-like events associated with wall 1 carry a large Reynolds shear stress beyond the centreline of the duct, their negative contribution to the Reynolds shear stress near wall 2 is negligible.

Wei & Willmarth's suggestion that the two wall regions continuously exchange spanwise vorticity is not supported by figure 20 which contains plots of the average value of $\Omega_z \equiv \partial V/\partial x - \partial U/\partial y$ as well as $\tilde{\bar{\Omega}}_z$, the contribution to $\bar{\Omega}_z$ from the heated

region. This latter contribution is negative (although the magnitude is quite small, seen in the inset of figure 20) up to $y/h \approx 1.5$, reflecting the intrusion across the centreline of fluid of opposite vorticity to that in the region $1 < y/h < 2$. This seems consistent with the negative sign of $(\overline{u^+v^+})_{II}$ up to $y/h \approx 1.5$ (figure 19). In the region $1,5 \lesssim y/h \lesssim 1.85$, the contribution to $\bar{\Omega}_z$ is positive (although its magnitude is quite small), possibly owing to the contribution from wall 2 sweeps.

6. Active motion and inactive motion

To test the hypothesis that, near solid boundaries, the high-Reynolds-number turbulence structure differs significantly from that at low Reynolds numbers, WW examined spectra of u and v, (they also considered power spectra of the product uv; they are not considered here as they are less relevant in the present context than the co-spectra). Spectra were presented near $y^+ = 15$ for the three lower Re values in their experiments, generally in the form $\omega^+\phi_u$ or $\omega^+\phi_v$ *vs.* $\log\omega^+$, where $\omega^+ \equiv \omega\nu/U_\tau^2$ and the normalization for the spectral density ϕ is such that

$$\int_0^\infty \phi_u \,\mathrm{d}\omega^+ = u'^{+2} \quad \text{or} \quad \int_0^\infty \phi_v \,\mathrm{d}\omega^+ = v'^{+2}.$$

At this location, the energy-containing part of ϕ_v showed a significant variation with Re commensurate with the increase in v'^+ with Re. The energy containing part of ϕ_u did not change appreciably with Re, in agreement with the relatively small variation in u'^+ at $y^+ \approx 15$. It was noted, however, that the high-wavenumber part of ϕ_u increases with Re 'demonstrating that, in non-dimensional terms, smaller eddies appear at higher Reynolds number which is consistent with the notion of increased vortex stretching'. It was emphasized that the increase in ϕ_u at large ω^+ was quite small and did not therefore affect u'^+ at that location.

Here we present measured and DNS spectra of u, v and the co-spectrum Co_{uv}. The measured spectra are at $y^+ \approx 32$, the smallest location at which measurements could be made at the highest Reynolds number. This location also falls approximately in the logarithmic region at all values of Re. The DNS spectra are at $y^+ = 40$, a location which also falls in the logarithmic region or, (perhaps more appropriately, as discussed by Spalart 1988) near the local minimum in $(y^+ \,\mathrm{d}\bar{U}^+/\mathrm{d}y^+)$. The normalization in figures 21 and 22 is as shown in (1). It should be noted that this presentation would be equivalent to using either ω^+ (for experimental data) or $k_1\eta$ provided scaling on wall variables is assumed to apply in the inner region. From $\bar{U} = U_\tau f(y^+)$, it follows immediately that $k_1^+ = \omega^+ f^{-1}$ while it is easy to show that $k_1 = (k_1\eta)\,g^{\frac{1}{4}}$ where $\bar{\epsilon}^+ = g(y^+)$. If the functions f and g are universal, then the equivalence between k_1^+ and either ω^+ or $k_1\eta$ would be fully justifiable. The dependence of f on Re is small (figure 3) while the dependence of g on Re is mainly confined to $y^+ \lesssim 15$ (figure 12). On the other hand, the use of k_1^+ is fully consistent with using $k_1 y$ when spectra are compared at the same y^+ value, since $k_1^+ \equiv (k_1 y)/y^+$; this equivalence does not hinge on the validity of wall scaling.

When the spectra are plotted in the form $k_1^+\phi$ (in this type of plot, the areas under the curves are proportional to the contributions to the total energy from the wavenumber bands) or $-k_1^+ Co$ *vs.* $\log k_1^+$, it is evident that, for both the measured and DNS spectra, the major influence of Re is at relatively small k_1^+ rather than large k_1^+. The scatter and resolution at small k_1^+ are larger for the DNS than for the measured spectra.

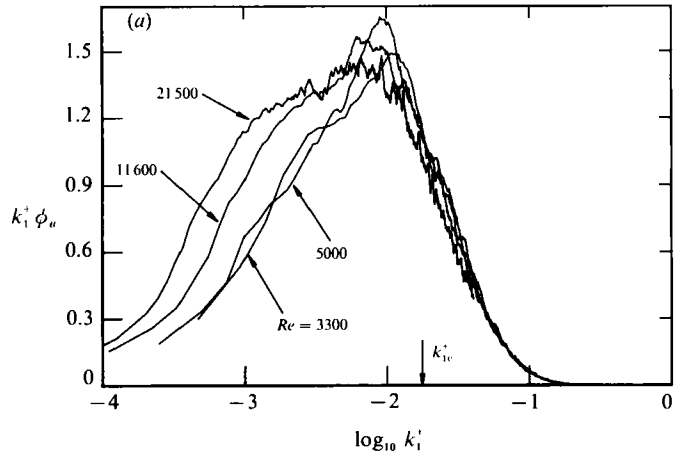

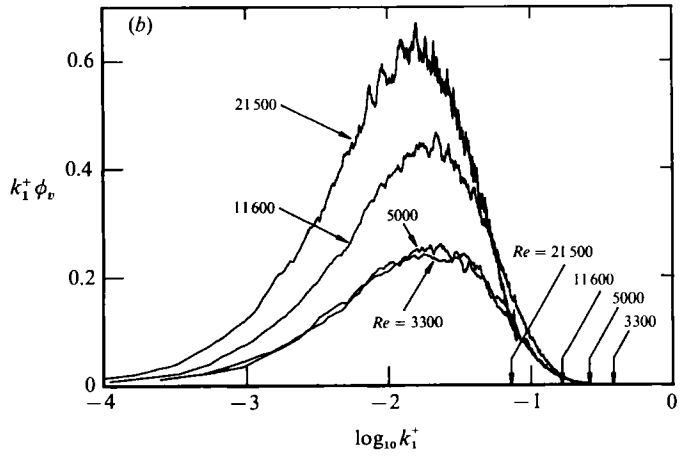

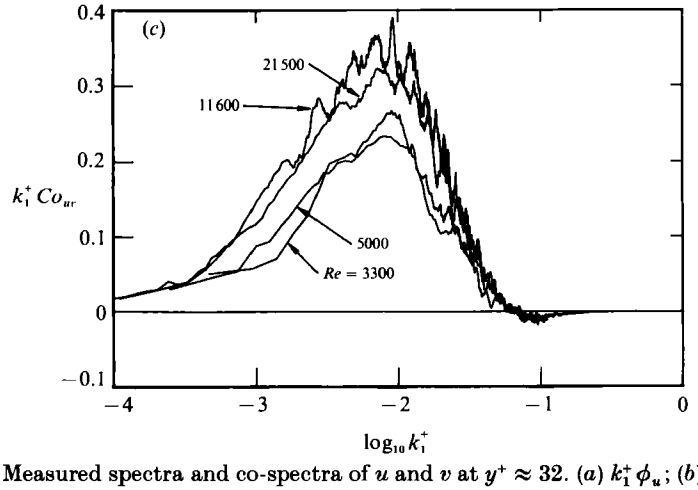

FIGURE 21. Measured spectra and co-spectra of u and v at $y^+ \approx 32$. (*a*) $k_1^+ \phi_u$; (*b*) $k_1^+ \phi_v$; (*c*) $-k_1^+ Co_{uv}$. Arrows on the abscissa in (*b*) represent the normalized wavenumbers which correspond to the wire length at the various Re.

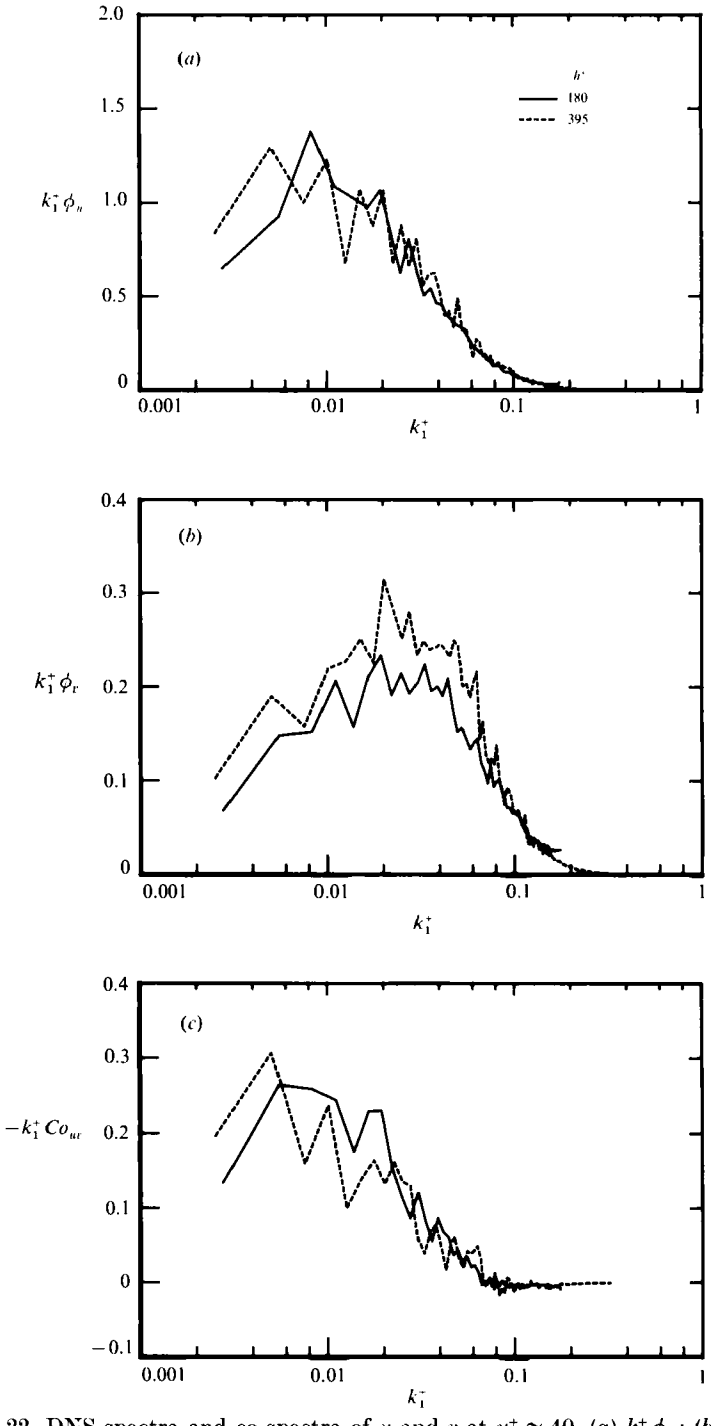

FIGURE 22. DNS spectra and co-spectra of u and v at $y^+ \approx 40$. (a) $k_1^+\phi_u$; (b) $k_1^+\phi_v$; (c) $-k_1^+Co_{uv}$.

Figure 21 (a) shows that virtually all the Reynolds number variation occurs to the left of the peak. A wavenumber k_{1c}^+ can be identified (figure 21 a) for which the Re dependence is small when $k_1^+ > k_{1c}^+$. If the area under the spectrum in the region $k_1^+ < k_{1c}^+$ is designated by A_e, and the total area by A, the ratio A_e/A is a measure of the

contribution to u'^{+2} from the range $k_1^+ < k_{1c}^+$. For the present conditions, A_e/A increases from 0.55 ($Re = 3300$) to 0.72 ($Re = 21500$). The peak in figure 21(*a*) broadens as Re increases, a trend consistent with the possible onset of a k_1^{-1} behaviour, at least when the Reynolds number becomes sufficiently large. Although WW presented their u spectrum on a $\omega^+\phi$ *vs.* $\log\omega^+$ plot, no data were shown for $\log\omega^+ \lesssim -1.8$ (this corresponds to $\log k_1^+ \lesssim -2.7$ at $y^+ \approx 15$), a region which could contribute to as much as 25% to u'^{+2}. For the DNS u-spectra (figure 22*a*) the increase is confined to small k_1^+.

Figure 21(*b*) shows that the energy containing part of the v-spectrum increases only marginally between $Re = 3300$ and 5000. There is also a small increase in the DNS spectra (figure 22*b*) between $Re = 3300$ and $Re = 7900$, commensurate with the increase in v'^{+2}. The significant increase in the measured ϕ_v (figure 21*b*) at the two larger Reynolds numbers is probably an error due to the unlikely increase in v'^+ (figure 5) at $Re = 11600$ and 21500 for $y^+ \lesssim 100$. The arrows on the abscissa of figure 21(*b*) represent the normalized wavenumbers which correspond to the wire length (actually the average length of the two wires of the X-probe) at the various Re. It is clear that the spatial resolution is adequate (except perhaps at $Re = 21500$ where there may be an attenuation in v'^{+2} of about 5%) and cannot therefore explain the anomalous increase in v'^{+2} shown in figure 5.

At sufficiently large wavenumbers ($k_1^+ \approx 0.1$), the cospectrum Co_{uv} changes sign (figure 21*c*). This feature, also observed in the DNS data, (figure 22*c*, also figure 6) for the uv cospectrum, indicates that small scales can provide a very small positive contribution to $\overline{uv}$ and hence to the negative production of turbulent energy. The part of the co-spectrum which contains most of the Reynolds shear stress increases with Re (figure 21*c*). This trend is less evident for the DNS co-spectra (figure 22*c*) owing mainly to the small overall increase in Re. There is nevertheless a small increase at small k_1^+, which accounts for the increase in the magnitude of $\overline{u^+v^+}$ with Re. The Reynolds number evolution of Co_{uv} indicates that the concept of an active motion, which contributes practically all the Reynolds shear stress in the inner region, is reasonable only if it is assumed that the active motion depends on the Reynolds number. The increase in ϕ_v with Re (figure 22*b*) confirms this assumption.

The concept of an Re-independent active motion is perhaps more tenable at the largest values of Re, considering the relatively small difference in Co_{uv} between $Re = 11600$ and 21500. The inactive motion, consisting of the large-scale vorticity field and the irrotational pressure fluctuations of the outer region (Townsend 1961; Bradshaw 1967) should continue to affect the low wavenumber parts of the u (and w) spectra as Re increases further. (In the context of duct flow, the outer region would include the large-scale vortical field and pressure fluctuations associated with the opposite wall.) The magnitudes (in the inner region) of u'^{+2} (and w'^{+2}) should therefore continue to increase with Re while $\overline{u^+v^+}$ and v'^{+2} should be relatively unchanged. Available data, obtained mostly in the boundary layer (Bradshaw 1967; Perry *et al.* 1986, 1987; Spalart 1988) suggest that the major effect is indeed on u'^{+2} and w'^{+2}. Expressions for the normal stresses in the turbulent wall region have been obtained using different approaches, by Townsend (1976), and Perry *et al.* (1986, 1987, 1990). By integrating over all the spectral regions (i.e. inactive motion + active motion + small scale), Perry *et al.* obtained

$$u'^{+2} = B_1 - A_1 \ln\left(\frac{y^+}{\delta^+}\right) - V_1(y^+), \tag{5}$$

$$v'^{+2} = A_3 - V_2(y^+), \tag{6}$$

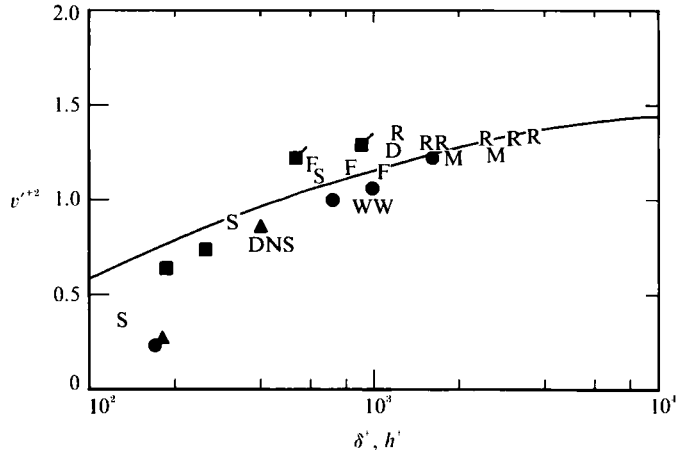

FIGURE 23. Dependence of v'^{+2} on the Reynolds number at $y/h = 0.1$ (duct) and $y/\delta = 0.1$ (boundary layer). Duct: Experiments – ■, present (tagged symbols are explained in the text); ○, Wei & Willmarth (1989); ▲, DNS. Boundary layer: letters and curve are taken from Perry *et al.* (1990).

with an expression for w'^{+2} similar to (5). here A_1 and A_3 are universal constants while B_1 is a constant characteristic of the large-scale motion, viz. it may be different in pipe, duct and boundary-layer flows. The functions V_1 and V_2, which reflect the viscous cut-off effect (or an energy deficiency due to a finite Reynolds number) did not appear in Townsend's (1976) attached eddy result. At a fixed value of y^+, relation (6) predicts that v'^{+2} should be constant, independent of the flow. This result is strictly valid however when the Reynolds number is sufficiently large for the existence of a range where y^+ is greater than about 100 and y/h is less than about 0.1. This is not satisfied by most of the present data. There is correspondingly no evidence in figures 5 and 10 that v'^{+2} is constant at the same y^+ (the choice of y^+ is not critical in view of the plateau in v'^{+2}). It is nevertheless of interest to determine whether the present v'^{+2} data becomes compatible with relation (ii) as h^+ increases. Perry *et al.* (1990) plotted carefully selected boundary-layer data for v'^{+2} at $y/\delta = 0.1$ as a function of δ^+. The selection aimed to eliminate X-wire data with spatial resolution or cone angle inadequacies or data which failed to yield a correct $\overline{uv}$. Also included in their plot was the DNS data of Spalart (1988). Figure 23, which is adapted from figure 13 of their paper, includes thc present duct data. The curve is the analytical result given by Perry *et al.* (1990). Apart from the two tagged points (they are doubtful as they correspond to $Re = 11600$ and 21500), the duct data tend to merge into the boundary layer data when h^+ is sufficiently large. Note that $h^+ \approx 1000$ corresponds to $Re \approx 20000$ which is roughly when Reynolds-number similarity is approximately achieved in the outer region of the duct.

It could be argued that the form of (6) is not necessarily exact as there are no strong arguments to suggest that v is completely unaffected by the inactive motion. Bradshaw (1967) argued that the v component of 'any sort of large scale motion is small at distances from the wall small compared with a longitudinal wavelength, as follows from the continuity equation'. The data he presented showed however that, at low wavenumbers, ϕ_v is not as universal as Co_{uv}.

It would be incorrect to attribute the strong Reynolds-number dependence of the present data solely to the inactive motion (the Reynolds-number dependence in the 'outer region' of a duct is in any case known to be much smaller than in a boundary

layer) in view of the small disparity between the lengthscales ν/U_τ and h. The marked evolution of ϕ_v (or $\overline{v'^{+2}}$) and Co_{uv} (or $\overline{u^+v^+}$) with h^+ contrasts with the more localized low wavenumber variation of ϕ_u, reflecting the difference in the scales which govern u and v (or uv).

7. Comparison with the boundary layer

Although the contribution from quadrant II is negligible for $y/h \gtrsim 1.25$ (figure 19), it is of interest to compare the ratio $(\overline{uv})_{\rm II}/(\overline{uv})_{\rm IV}$, the ratio of contributions to $\overline{uv}$ from quadrants II and IV, in a duct with that in a boundary layer, given that quadrant II events protrude a significant distance beyond the duct centreline at low Reynolds numbers.

Lu & Willmarth (1973) compared their boundary-layer measurements ($R_\theta = 4230$) of $(\overline{uv})_{\rm II}/(\overline{uv})_{\rm IV}$ with those of Wallace *et al.* (1972) in a duct ($R = 3575, R_\theta = 360$). The comparison (figure 15 of their paper) showed a significant difference between the wall regions of these two flows, $(\overline{uv})_{\rm II}/(\overline{uv})_{\rm IV}$ continuing to increase with decreasing y^+. Speculatively, the difference was attributed to either a difference in Reynolds number or, more probably, errors in measurement. None of the results presented in the previous sections suggest that a difference of the order observed by Lu & Willmarth is possible. It seemed important therefore to compare the near-wall behaviour of $(\overline{uv})_{\rm II}/(\overline{uv})_{\rm IV}$ for these two flows. The Reynolds number at which such a comparison should be made requires comment. It is reasonable to suppose that each of these flows will achieve approximate Reynolds-number similarity above a particular Reynolds number, $R_{\rm cr}$ say. Available data suggest that $R_{\rm cr}$ can be identified with $R_\theta \approx 3000$–5000 for the boundary layer and with $Re \approx 2 \times 10^4$ in the duct. It would seem reasonable to compare the two flows at Reynolds numbers equal to or greater than $R_{\rm cr}$. At such Reynolds numbers, however, it would be difficult to make reliable X-probe measurements in the near-wall region. As the most accurate data in this region is provided by the DNS, the ratio $(\overline{uv})_{\rm II}/(\overline{uv})_{\rm IV}$ was computed for the boundary-layer data ($R_\theta \approx 300, \delta^+ \approx 160$) of Spalart (1988) and the present duct data ($R_\theta \approx 300, h^+ \approx 180$). One disadvantage of choosing this low Reynolds number (probably close to the lower limits for the flows to be considered turbulent), is that low-Reynolds-number effects are important in both flows. If the 'geometry effect' is largest at this Reynolds number, any difference between the duct and the boundary layer should presumably also be largest.

The comparison, shown in figure 24, indicates that the two distributions follow each other closely in the region $y^+ \lesssim 25$. In particular, the ratio crosses unity at $y^+ \approx 13$ (a detailed discussion of the near-wall behaviour of the contributions from all quadrants to $\overline{uv}$ can be found in Kim *et al.* 1987) for both the duct and the boundary layer, thus reflecting the dominance of sweeps over ejections in the sublayer and the inner part of the buffer layer. Notwithstanding the small range of R_θ in figure 24, Lu & Willmarth's (1973) suggestion that there may be significant differences between the near-wall values of $(\overline{uv})_{\rm II}/((\overline{uv})_{\rm IV}$ in these two flows seems unlikely.

The region ($y^+ \gtrsim 40$) over which the two distributions differ is nonetheless significant as a proportion of the duct half-width. Over most of this region, the ratio is smaller for the duct than for the boundary layer. Examination of the individual $(\overline{u^+v^+})_{\rm II}$ and $(\overline{u^+v^+})_{\rm IV}$ distributions shows that this behaviour is due mainly to $(\overline{u^+v^+})_{\rm IV}$ being larger in the duct than in the boundary layer; the magnitude of $(\overline{u^+v^+})_{\rm II}$ is comparable in the two flows. This seems consistent with excursions of relatively high-speed ($u > 0$) fluid associated with the wall 2 shear layer across the centreline

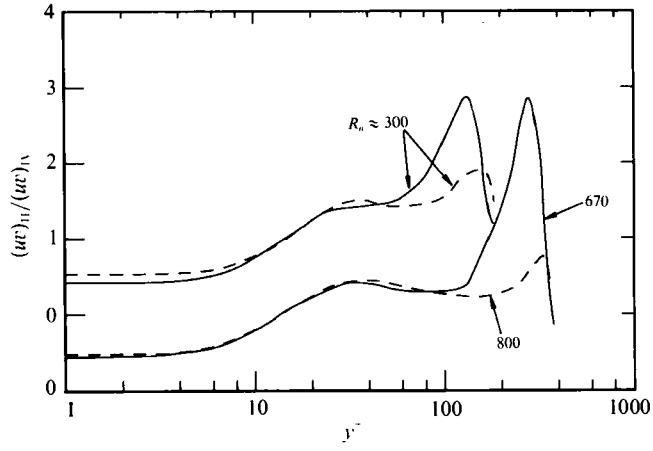

FIGURE 24. Comparison between boundary layer and the duct of the ratio $(\overline{uv})_{II}/(\overline{uv})_{IV}$. ——, boundary layer (Spalart 1988); – – –, duct.

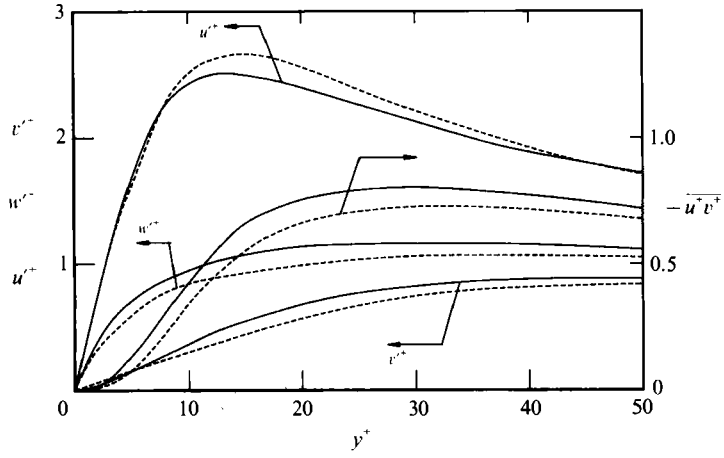

FIGURE 25. Comparison of u'^+, v'^+, w'^+ and $-\overline{u^+v^+}$ between ——, boundary layer (Spalart 1988) and – – –, duct at $R_\theta \approx 300$.

($v < 0$). It is consistent with the earlier association between temperature in the wall 2 region and the sweep-quadrant motion of that wall.

When the comparison is extended to higher Reynolds numbers, the distributions, shown with a displaced origin in figure 24, are now in agreement for $y^+ \lesssim 100$. The values of R_θ are larger for the duct ($R_\theta = 800$) than the boundary layer but the values of the Kármán number are not very different: $h^+ \approx 390, \delta^+ \approx 380$. In the region $y^+ \lesssim 40$, the duct and boundary-layer follow approximately the same distribution, irrespective of Reynolds number. It would appear that in this region, the ratio $(\overline{uv})_{II}/(\overline{uv})_{IV}$ does not depend on either the flow or the Reynolds number.

A comparison between distributions of u', v', w' and $\overline{uv}$ in the near-wall regions of these two flows at similar values of R_θ (or, perhaps more appropriately, for similar values of Kármán number) indicates that there are some differences (figure 25). While these differences may decrease as the Reynolds number increases, they may not entirely disappear, at least for u' and w', as the effect of the inactive motion differs in the two flows.

8. Conclusions and concluding comments

1. Both the DNS and the experimental duct data show significant low-Reynolds-number effects, comparable to those already reported for the boundary layer by Spalart (1988). In particular, the near-wall region data corroborate Wei & Willmarth's (1989) contention that scaling on wall variables is not correct, although the various wall-normalized quantities that we have considered have exhibited different Reynolds-number dependences. For example, the DNS data show that the effect of Re on the r.m.s. value of w appears to be greater than on u or v. The effect of Re on the average production and dissipation of turbulent energy is generally small except for the significant increase of $\bar{\epsilon}$ with Re within the sublayer. The ratio of contributions to the Reynolds shear stress from the second and fourth quadrants is essentially unaffected by the Reynolds number.

2. Whereas u'^+ has a clear peak at approximately the same y^+ location ($y^+ \approx 15$), the peaks in v'^+ or $\overline{u^+v^+}$ are much broader and increase with the Reynolds number h^+. The $h^{+\frac{1}{2}}$ increase in the location of $(\overline{u^+v^+})_{\max}$ is as reported by Sreenivasan (1990) who reviewed boundary-layer, pipe and duct flow data.

3. Consistent with the observed effects of h^+ on v'^+ and $\overline{u^+v^+}$, changes with h^+ in the v-spectrum or the uv co-spectrum are more significant than those in the u spectrum. The latter are primarily confined to low wavenumbers. Wei & Willmarth's claim that the increased stretching of longitudinal vortices can partly explain low-Reynolds-number effects near the wall is supported by the observed changes in v'^+ and ϕ_y (as expected, the increase of ϕ_u with Re is relatively unimportant). The claim should also apply to the boundary layer. Indeed, it is directly supported by Spalart's observations that, near the wall, $\omega_x'^+$, the normalized r.m.s. streamwise vorticity component increases as the Reynolds number increases. Note that the increase in the average turbulent energy dissipation near the wall (figure 12) implies a corresponding increase in mean square vorticity $\overline{\omega^2}$ since $\bar{\epsilon} = \nu\overline{\omega^2}$ (by assuming homogeneous turbulence).

It would be improper to attribute the low-wavenumber variations of ϕ_u with Re entirely to the inactive motion in view of the significant evolution of ϕ_v and especially Co_{uv}. Spalart discussed low-Reynolds-number effects in the boundary layer in the context of the contributions from the inactive motion but there is evidence of a non-negligible variation in the uv co-spectra at low wavenumbers which implies a Reynolds number dependent active motion. While the contribution from the inactive motion cannot be ignored at small Reynolds numbers, its determination would be difficult, perhaps impossible. At these Reynolds numbers, the small disparity between the lengthscales h and ν/U_τ makes the distinction between active and inactive motions ambiguous. The data of figure 21 (*c*) suggest that the variation in Co_{uv} may decrease with increasing h^+, so that the contribution from the inactive motion (primarily to u'^{+2} and w'^{+2}) may be more easily determined at larger values of h^+ than considered here.

4. Results of §6 provide relatively direct evidence of the geometry effect in the duct. Fluid from the slightly heated wall region can reach the near-wall region of the opposite wall. The penetration depth and frequency of occurrence of thermal excursions increase as the Reynolds number decreases. Since the magnitude of this frequency is small, these excursions do not make a significant contribution to $\overline{uv}$ in the inner region. In particular, we have found no evidence to support Wei & Willmarth's suggestion that opposite near-wall regions constantly exchange opposite-signed (spanwise) vorticity and shear stress. There is an indication,

however, that when heated fluid is detected on the opposite side of the centreline from the heated wall, it is generally related to a sweep-type motion associated with the unheated wall. This is reflected in the smaller value of $(\overline{uv})_{II}/(\overline{uv})_{IV}$, the ratio of the contributions from quadrants II and IV to $\overline{uv}$, in the outer region of the duct than in the boundary layer.

5. Although we have found no evidence that fluid from one wall significantly contributes to the Reynolds shear stress near the opposite wall, it would be incorrect to view the interaction between opposite shear layers of the duct as being confined solely to a small region which straddles the centreline. This view would not be consistent with the comparison at small R_θ between the duct and the boundary layer (figure 24).

R.A.A. and L.W.B.B. are grateful for the support of the Australian Research Council and the Center for Turbulence Research.

REFERENCES

BRADSHAW, P. 1967 'Inactive' motion and pressure fluctuations in turbulent boundary layers. *J. Fluid Mech.* **30**, 241–258.

BRADSHAW, P., DEAN, R. B. & MCELIGOT, D. M. 1973 Calculation of interacting turbulent shear layers: Duct flow. *J. Fluids Engng* **95**, 214–219.

CHEN, C.-H. P. & BLACKWELDER, R. F. 1978 Large-scale motion in turbulent boundary layer: A study using temperature contamination. *J. Fluid Mech.* **89**, 1–31.

COLES, D. 1978 A model for flow in the viscous sublayer. In *Lehigh Workshop on Coherent Structure in Turbulent Boundary Layers* (ed. C. R. Smith & D. E. Abbott), pp. 462–475. Lehigh University.

COMTE-BELLOT, G. 1965 PhD thesis, University of Grenoble (trans. P. Bradshaw).

DEAN, R. B. 1978 Reynolds number dependence of skin friction and other bulk flow variables in two-dimensional rectangular duct flow. *J. Fluids Engng* **100**, 215–223.

DEAN, R. B. & BRADSHAW, P. 1976 Measurements of interacting turbulent shear layers in a duct. *J. Fluid Mech.* **78**, 641–676.

EL TELBANY, M. M. M. & REYNOLDS, A. J. 1980 Velocity distributions in plane turbulent channel flows. *J. Fluid Mech.* **100**, 1–29.

EL TELBANY, M. M. M. & REYNOLDS, A. J. 1981 Turbulence in plane channel flows. *J. Fluid Mech.* **111**, 283–318.

HUFFMAN, G. D. & BRADSHAW, P. 1972 A note on von Kármán's constant in low Reynolds number turbulent flows. *J. Fluid Mech.* **53**, 45–60.

JOHANSSON, A. V., ALFREDSSON, P. H. & KIM, J. 1987 Shear layer structures in near-wall turbulence. *Proc. 1987 Summer Program.* Center for Turbulence Research, Rep. CTR-587, pp. 237–251.

KIM, J. & MOIN, P. 1986 The structure of the vorticity field in turbulent channel flow. *J. Fluid Mech.* **162**, 339–363.

KIM, J., MOIN, P. & MOSER, R. 1987 Turbulence statistics in fully developed channel flow at low Reynolds number. *J. Fluid Mech.* **177**, 133–166.

KLINE, S. J. & ROBINSON, S. K. 1990 Quasi-coherent structures in the turbulent boundary layer. Part I: Status report on a community-wide summary of the data. In *Near-Wall Turbulence* (ed. S. J. Kine & N. H. Afgan), pp. 200–217. Hemisphere.

KREPLIN, H. P. & ECKELMANN, H. 1979 Behavior of the three fluctuating velocity components in the wall region of a turbulent channel flow. *Phys. Fluids* **22**, 1233.

LAUFER, J. 1950 Investigation of turbulent flow in a two-dimensional channel. *NACA Rep.* 1053.

LU, S. S. & WILLMARTH, W. W. 1973 Measurements of the structure of the Reynolds stress in a turbulent boundary layer. *J. Fluid Mech.* **60**, 481–511.

LYONS, S. L., HANRATTY, T. J. & MCLAUGHLIN, J. B. 1989 Turbulence-producing eddies in the viscous wall region. *AIChE J.* **35**, 1962–1974.

MANSOUR, N. N., KIM, J. & MOIN, P. 1989 Near-wall $k-\epsilon$ turbulence modelling, *AIAA J.* **27**, 1068–1073.

MOIN, P. & SPALART, P. R. 1987 Contributions of numerical simulation data bases to the physics, modeling, and measurement of turbulence. *NASA TM* 100022. NASA-Ames Research Center.

MURLIS, J., TSAI, H. M. & BRADSHAW, P. 1982 The structure of turbulent boundary layers at low Reynolds numbers. *J. Fluid Mech.* **122**, 13–56.

PATEL, V. C. & HEAD, M. R. 1969 Some observations on skin friction and velocity profiles in fully developed pipe and channel flows. *J. Fluid Mech.* **38**, 181–201.

PERRY, A. E., HENBEST, S. & CHONG, M. S. 1986 A theoretical and experimental study of wall turbulence. *J. Fluid Mech.* **165**, 163–199.

PERRY, A. E., LI, J. D., HENBEST, S. M. & MARUSIC, I. 1990 The attached eddy hypothesis in wall turbulence. In *Near-Wall Turbulence* (ed. S. J. Kline & N. H. Afgan), pp. 715–735. Hemisphere.

PERRY, A. E., LIM, K. L. & HENBEST, S. M. 1987 An experimental study of the turbulence structure in smooth- and rough-wall boundary layers. *J. Fluid Mech.* **177**, 437–466.

PURTELL, L. P., KLEBANOFF, P. S. & BUCKLEY, F. T. 1981 Turbulent boundary layer at low Reynolds number. *Phys. Fluids* **24**, 802–811.

REYNOLDS, A. J. & EL TELBANY, M. M. M. 1982 Velocity and eddy-diffusivity distributions in the buffer region of turbulent wall flow. *Phys.-Chem. Hydrodyn.* **3**, 127–137.

SABOT, J. & COMTE-BELLOT, G. 1976 Intermittency of coherent structures in the core region of fully developed turbulent pipe flow. *J. Fluid Mech.* **74**, 767–796.

SHAH, D. A. 1988 Scaling of the 'bursting' and 'pulse' periods in wall-bounded turbulent flows. PhD thesis, University of Newcastle, Australia.

SPALART, P. R. 1988 Direct simulation of a turbulent boundary layer up to $R_\theta = 1410$. *J. Fluid Mech.* **187**, 61–98.

SREENIVASAN, K. R. 1990 The turbulent boundary layer. In *Frontiers in Experimental Fluid Mechanics* (ed. M. Gad-el-Hak), pp. 159–210. Springer.

SUBRAMANIAN, C. S., RAJAGOPALAN, S., ANTONIA, R. A. & CHAMBERS, A. J. 1982 Comparison of conditional sampling and averaging techniques in a turbulent boundary layer. *J. Fluid Mech.* **123**, 335–362.

SUZUKI, Y. & KASAGI, N. 1990 Evaluation of hot-wire measurements in turbulent wall shear flows using a direct numerical simulation data base. In *Engineering Turbulence Modelling and Experiments* (ed. W. Rodi & E. N. Ganic), pp. 361–370. Elsevier.

TEITEL, M. & ANTONIA, R. A. 1990 The interaction region in a turbulent duct flow. *Phys. Fluids* A **2**, 808–813.

TOWNSEND, A. A. 1961 Equilibrium layers and wall turbulence. *J. Fluid Mech.* **11**, 97–120.

TOWNSEND, A. A. 1976 *The Structure of Turbulent Shear Flow*, pp. 150–156. Cambridge University Press.

WALLACE, J. M. 1982 On the structure of bounded turbulent shear flow: A personal view. In *Developments in Theoretical and Applied Mechanics* (ed. T. J. Ching), vol. 11, pp. 509–521. Department of Mechanical Engineering, University of Alabama-Huntsville.

WEI, T. & WILLMARTH, W. W. 1989 Reynolds-number effects on the structure of a turbulent channel flow. *J. Fluid Mech.* **204**, 57–95.